

# A comprehensive CCD photometric study of the open cluster NGC 2421

R. K. S. Yadav<sup>1\*</sup> and Ram Sagar<sup>2†</sup>

<sup>1</sup>*Inter-University Centre for Astronomy and Astrophysics, Ganeshkhind, Pune 411 007, India*

<sup>2</sup>*State Observatory, Manora Peak Nainital 263 129, India*

Accepted ———. Received ———;

## ABSTRACT

We present the *UBVRI* CCD photometry in the region of the open cluster NGC 2421. Radius of the cluster is determined as  $\sim 3'.0$  using stellar density profile. Our Study indicates that metallicity of the cluster is  $Z \sim 0.004$ . The reddening  $E(B - V) = 0.42 \pm 0.05$  mag is determined using two colour ( $U - B$ ) versus ( $B - V$ ) diagram. By combining the 2MASS *JHK* data with the optical data we determined  $E(J - K) = 0.20 \pm 0.20$  mag and  $E(V - K) = 1.15 \pm 0.20$  mag for this cluster. Colour-excess diagrams show normal interstellar extinction law in the direction of the cluster. We determined the distance of the cluster as  $2.2 \pm 0.2$  Kpc by comparing the ZAMS with the intrinsic CM diagram of the cluster. The age of the cluster has been estimated as  $80 \pm 20$  Myr using the stellar isochrones of metallicity  $Z = 0.004$ . The mass function slope  $x = 1.2 \pm 0.3$  has been derived by applying the corrections of field stars contamination and data incompleteness. Our analysis indicate that the cluster NGC 2421 is dynamically relaxed.

**Key words:** Star cluster - individual: NGC 2421 - stars: Interstellar extinction, luminosity function, mass function, mass segregation - HR diagram.

## 1 INTRODUCTION

The investigation of young open star clusters provides us a powerful tool to understand the structure and history of star formation in our Galaxy. In order to fully exploit the information provided by open clusters we must know their accurate ages, distances, reddenings, metal abundances and stellar contents. For this, multicolour CCD photometric observations have proved to be very useful. With the development of more accurate stellar models it has been possible to provide a better estimate of the cluster ages simply by comparing theoretical isochrones with the observed CCD colour-magnitude (CM) diagrams. So, In this paper we have considered an open cluster NGC 2421 with the aim of presenting new accurate CCD photometry. From this photometry we select photometric members and derive several fundamental parameters, such as distance, interstellar reddening, metallicity and age as well as luminosity and mass function.

The young open cluster NGC 2421 = C0734–205 ( $\alpha_{2000} = 07^h 36^m 16^s$ ,  $\delta_{2000} = -20^d 36' 44''$ ;  $l = 236^\circ.24$ ,  $b = 0^\circ.08$ ) is classified as a Trumpler class I2m by Ruprecht (1966). This cluster was first studied by Moffat & Vogt (1975) photoelectrically and derived a distance of about 1.87

Kpc having  $E(B - V) = 0.47 \pm 0.05$  mag and age less than  $10^7$  years. Ramsay & Pollacco (1992) also studied this cluster using CCD photometry and found a colour excess  $E(B - V) = 0.49 \pm 0.03$  mag but a distance of 2.75 Kpc. To our knowledge no other studies have been carried out for the cluster NGC 2421 so far.

The layout of the paper is as follows. In Sec. 2 we briefly describe the observations and data reduction strategies as well as comparison with the previous photometry. Sec. 3 is devoted on the detailed analysis of the present photometric data for the determination of cluster parameter. Finally, Sec. 4 summarizes the main results of the paper.

## 2 OBSERVATIONS AND DATA REDUCTION

*UBVRcIc* CCD photometry was performed for the cluster NGC 2421 on 24/25 February 2003 at State Observatory Naini Tal with the 104-cm telescope (f/13) and a 2K×2K CCD (24- $\mu$ m pixels). The scale was  $0''.36$  pixel<sup>-1</sup>, giving 12.6 on a side. The read out noise for the system was 5.3 e<sup>-</sup>, while the gain was 10 e<sup>-</sup>/ADU. Table 1 lists the log of our CCD observations. To improve the S/N ratio, observations were made in 2×2 pixel binning mode while 2 to 3 deep exposures were taken for the accurate photometric measurements of faint stars. Many bias frames were taken during the

\* E-mail: rkant@iucaa.ernet.in

† E-mail: sagar@upsso.ernet.in

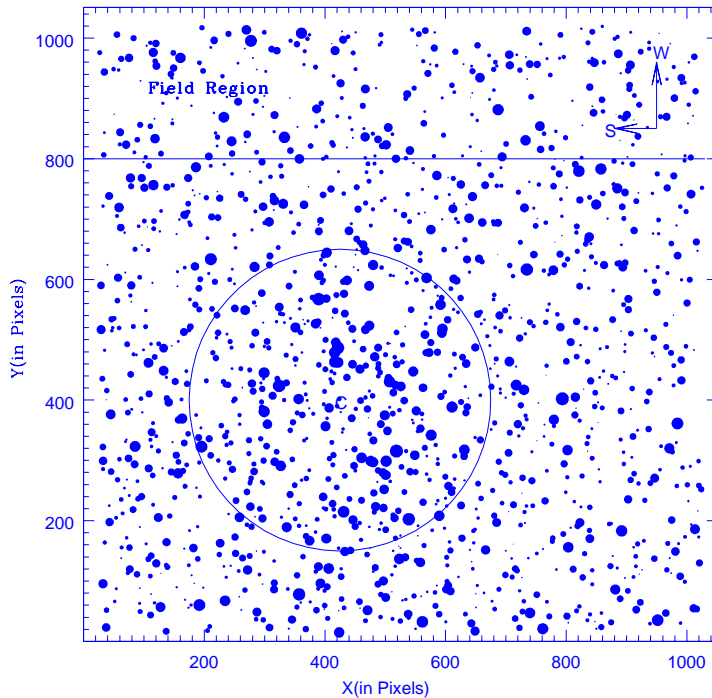


**Figure 1.** Finding chart of the stars in the cluster NGC 2421. The (X, Y) coordinates are in pixel units corresponding to  $0''.72$  on the sky. Direction is indicated in the map. Filled circles of different sizes represent brightness of the stars. Smallest size denotes stars of  $V \sim 20$  mag. Open circle having centre at 'C' in the chart represent the cluster size.

observations for removing the bias level in the images. Flat-field exposures were made of the twilight sky in each filter. Fig. 1 shows the finding chart for the stars brighter than  $V = 20$  mag in the cluster NGC 2421. We observed the standard area PG 1633+099 (Landolt 1992) several times during the night for the purpose of determination of atmospheric extinction coefficients and photometric calibration of the CCD system. The brightness and colour range of the standard stars are  $13 \leq V \leq 15$  and  $-0.2 \leq (V - I) \leq 1.1$  respectively. So, the standard stars in this area provide a good magnitude and colour range, essential to obtain reliable photometric transformation.

The data were reduced using the computing facilities available at Inter-University Centre for Astronomy and Astrophysics (IUCAA) Pune, India. Corrections to the raw data for bias and flat-fielding were performed using the standard IRAF routines. The CCD frames of the same exposure for a given filter were combined to improve the statistics of the faintest stars. Stellar magnitudes were obtained by using the DAOPHOT software (Stetson 1987, 1992) and conversion of the raw instrumental magnitudes into those of standard photometric system were done using procedures outlined by Stetson (1992). The instrumental magnitudes were derived through Point Spread Function (PSF) fitting using DAOPHOT. To determine the PSF, we used several well isolated stars for the entire frame. Several stars brighter than  $V = 11.0$  mag could not be measured as they saturated even on the shortest frame.

standard magnitude, the calibration equations derived using least square linear regression are as follows:

$$\begin{aligned} u &= U + 4.95 \pm 0.01 - (0.02 \pm 0.01)(U - B) + 0.62X \\ b &= B + 3.41 \pm 0.01 - (0.05 \pm 0.01)(B - V) + 0.28X \\ v &= V + 3.05 \pm 0.01 - (0.09 \pm 0.01)(B - V) + 0.17X \\ r &= R + 2.96 \pm 0.01 - (0.02 \pm 0.01)(V - R) + 0.12X \\ i &= I + 3.29 \pm 0.01 - (0.07 \pm 0.01)(R - I) + 0.10X \end{aligned}$$

where  $U, B, V, R$  and  $I$  are the standard magnitudes and  $u, b, v, r$  and  $i$  are the instrumental aperture magnitudes normalised for 1 second of exposure time and  $X$  is the airmass. We have ignored the second order colour correction terms as they are generally small in comparison to other errors present in the photometric data reduction. The errors in zero points and colour coefficients are  $\sim 0.01$  mag. The errors in magnitude and colour are plotted against  $V$  magnitude in Fig. 2 and the mean values of the errors are listed in Table 2. The final photometric data are available in electronic form at the WEBDA site <sup>‡</sup> and also from the authors.

## 2.1 Comparison with previous photometry

We have been obtained  $UBVRI$  photometry for  $\sim 1300$  stars down to  $V = 20$  mag in the region of NGC 2421. Ramsay et al. (1992) has also presented CCD  $UBV$  photometry for 98 stars. Fig 3 shows the plots of difference  $\Delta$  in  $V$ ,  $(B - V)$  and  $(U - B)$  with  $V$  magnitude. The average difference (in the sense: our values minus Ramsay et al.

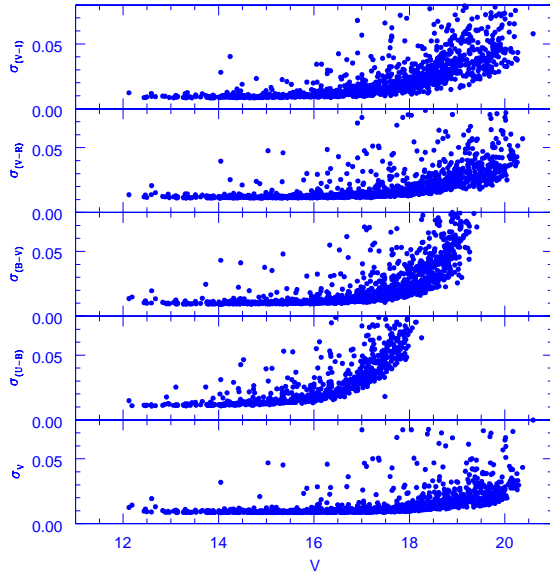


**Figure 2.** Photometric errors in magnitude and colour against  $V$  magnitude

**Table 1.** Journal of observations, with dates and exposure times for each passband.  $N$  denotes the number of stars measured in different passband.

Band	Exposure Time (in seconds)	Date	$N$
$U$	$1800 \times 2, 300 \times 2$	24/25 Feb 2003	770
$B$	$1200 \times 2, 240 \times 2$	„	1200
$V$	$900 \times 3, 180 \times 2$	„	1300
$R$	$500 \times 3, 120 \times 2$	„	1350
$I$	$300 \times 3, 60 \times 2$	„	1400

(1992)) alongwith their standard deviation are listed in Table 3. The comparison of ours and their  $V$  magnitudes shows a weak linear dependence of  $\Delta V$  with  $V$  which is shown by dotted line in Fig 3. The systematic difference of  $\sim -0.03$  mag is present in  $(B - V)$  colour without any dependence on

**Table 2.** Mean photometric errors in magnitude and colours in different magnitude bins

$V$	$\sigma_V$	$\sigma_{U-B}$	$\sigma_{B-V}$	$\sigma_{V-R}$	$\sigma_{V-I}$
12–13	0.014	0.012	0.014	0.011	0.010
13–14	0.010	0.012	0.011	0.012	0.009
14–15	0.010	0.014	0.011	0.012	0.010
15–16	0.010	0.017	0.011	0.012	0.011
16–17	0.010	0.025	0.013	0.013	0.014
17–18	0.011	0.038	0.017	0.016	0.015
18–19	0.019		0.018	0.025	0.035
19–20	0.023		0.025	0.035	0.054

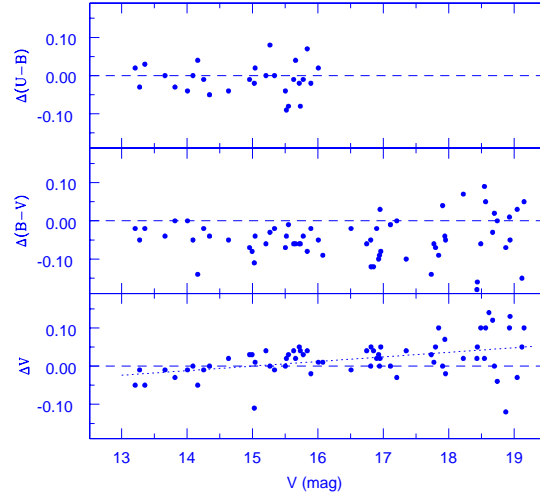


**Figure 3.** Comparison of our  $UBV$  photometry with the CCD photometry given by Ramsay et al. (1992). Dotted line represents a linear least square fitting to the data points.

**Table 3.** Comparison of the present CCD photometry with Ramsay et al. (1992). The difference ( $\Delta$ ) is always in the sense present minus comparison data. The mean along with their standard deviations in magnitude are based on  $N$  stars. Few deviated points are not included in the average determination.

$V$ range	$\langle \Delta V \rangle$ Mean $\pm\sigma(N)$	$\langle \Delta(B - V) \rangle$ Mean $\pm\sigma(N)$	$\langle \Delta(U - B) \rangle$ Mean $\pm\sigma(N)$
13.0 – 14.0	$-0.02 \pm 0.02(5)$	$-0.02 \pm 0.02(5)$	$0.00 \pm 0.02(5)$
14.0 – 15.0	$0.00 \pm 0.02(8)$	$-0.04 \pm 0.02(8)$	$0.00 \pm 0.04(8)$
15.0 – 16.0	$0.02 \pm 0.02(14)$	$-0.04 \pm 0.02(14)$	$-0.01 \pm 0.05(15)$
16.0 – 17.0	$0.02 \pm 0.02(12)$	$-0.05 \pm 0.04(9)$	
17.0 – 18.0	$0.02 \pm 0.04(10)$	$-0.04 \pm 0.04(9)$	
18.0 – 19.0	$0.03 \pm 0.04(8)$	$-0.00 \pm 0.05(10)$	

stellar magnitude while there is no significant difference or dependency seen in  $(U - B)$  colour with stellar magnitude.

### 3 DATA ANALYSIS

#### 3.1 Cluster radius

We used radial stellar density profile for the determination of cluster radius. For this, we selected the stars brighter than  $V = 20.0$  mag. The average stellar density was calculated in successive, 50 pixel wide annuli around the cluster center. The cluster center is determined iteratively by calculating average  $X$  and  $Y$  position of the stars within 400 pixels from an eye estimated center, until they converged to a constant value. In this way, we obtained the pixel coordinate of the cluster center as (425, 400) which is marked by 'C' in the Fig. 1. Fig. 4 shows the stellar surface density as a function

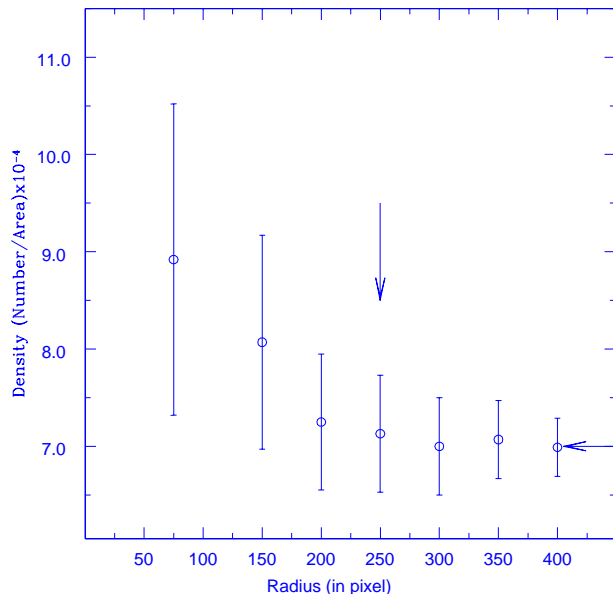


**Figure 4.** Star density as a function of radial distance from the center of the cluster with the stars brighter than  $V = 20.0$  mag. Errorbar denotes the error determined from sampling statistics ( $= \frac{1}{\sqrt{N}}$  where  $N$  is the number of stars used in the density estimation at that point). Horizontal and vertical arrows represent the density of the field stars and radius of the cluster respectively.

of distance from the cluster center. The density profile flattens at radius  $r = 250$  pixels. After  $r = 250$  pixels stellar density is merging into the field star density as indicated by horizontal arrow in Fig 4. The surface density of the field stars is derived as  $7 \times 10^{-4}$  per pixel<sup>2</sup>. In this way we estimated the radius  $3'.0$  for this cluster which is smaller than the value  $3'.5$  given by Mermilliod (1995).

We observed  $12'.5 \times 12'.5$  area towards the cluster NGC 2421 which is larger than the cluster radius and hence we have considered the stars as field stars which are having their position more than  $1.6$  cluster radius (see Fig. 1). The nearest boundary of the field region is about  $5'.0$  away from the cluster center in the west direction.

### 3.2 Apparent colour-magnitude diagrams of the cluster and field regions

Fig. 5 presents photometric colour-magnitude (CM) diagrams of the cluster and field region. To reduce the field star contamination in the CM diagrams, we used the stars within the cluster radius. The CM diagrams of the cluster extending down to  $V \sim 19.5$  mag except in  $V, (U - B)$  CM diagram where it is only up to  $V \sim 18$  mag. A main-sequence extending upto  $V = 19.0$  mag is clearly visible in the CM diagrams of the cluster. Contamination due to the field stars is evident, especially in the fainter parts of the CM diagrams. Ideally, one would like to eliminate the contamination from

**Table 4.** Frequency distribution of the stars in the  $V, (V - I)$  diagram of the cluster and field regions.  $N_B, N_S$  and  $N_R$  denote the number of stars in a magnitude bin blueward, along and redward of the cluster sequence respectively. The number of stars in the field regions are corrected for area differences.  $N_C$  (difference between the  $N_S$  value of cluster and field regions) denotes the statistically expected number of cluster members in the corresponding magnitude bin.

V range	Cluster region			Field region			$N_C$
	$N_B$	$N_S$	$N_R$	$N_B$	$N_S$	$N_R$	
12 - 13	0	4	2	0	0	3	4
13 - 14	0	13	7	0	0	6	13
14 - 15	0	26	10	0	8	10	18
15 - 16	0	38	14	0	10	19	28
16 - 17	1	52	10	0	22	15	30
17 - 18	21	57	11	0	24	24	33
18 - 19	24	47	11	1	37	35	10

the stars of the galactic field using the information contained in the proper motion/or radial velocity of the stars. Unfortunately, these studies are not available for this cluster and hence we are forced to base our analysis onto photometric arguments. We selected members by defining the binary sequence. It has been defined by shifting the blue envelope by  $0.80$  mag vertically, which is shown in the CM diagram of the cluster. In Table 4, we have listed the expected number of field stars using  $V, (V - I)$  CM diagram of the field region. From this Table we can estimate the frequency distribution of stars in different parts of the CM diagram. It is also clear that all photometric probable members can not be cluster members and non-members should be subtracted in the studies of cluster mass function etc. However, probable members located within a cluster radius from its center can be used to determine the cluster parameters, as they have relatively less field star contamination and this has been done in the sections to follow.

### 3.3 Colour-colour diagram

We present colour-colour (CC) diagram in Fig. 6. The ZAMS given by Schmidt-Kaler (1982) is shown by the continuous curve. It is clearly seen that this ZAMS is not fitting to the stars of A and F spectral type. Prominent excess in  $(U - B)$  colour is clearly visible for the stars of  $(B - V) > 0.50$  mag. This indicates that the cluster is metal deficient. The UV excess  $\delta(U - B)$  determined with respect to Hyades MS turns out to be  $\sim 0.15$  mag. We estimated  $[\text{Fe}/\text{H}] \sim -0.45$  ( $Z \sim 0.004$ ) adopting  $[\text{Fe}/\text{H}]$  versus  $\delta(U - B)$  relation by Carney (1979). Furthermore, we fitted the ZAMS given by Bertelli et al. (1994) for  $Z = 0.004$  to determine the reddening in the direction of cluster. The ZAMS of  $Z = 0.004$  which is shown by short dash lines in the two colour diagram fits well and provides the reddening  $E(B - V) = 0.42 \pm 0.05$  for this cluster. Our reddening estimate is in agreement with the earlier findings (see Sec. 1).

The nature of extinction law has also been studied by using the stars having spectral type earlier than A0. We selected these stars using CC and CM diagram and find that the stars with  $V \leq 15.0$  mag and  $(B - V) \leq 0.50$  mag are the

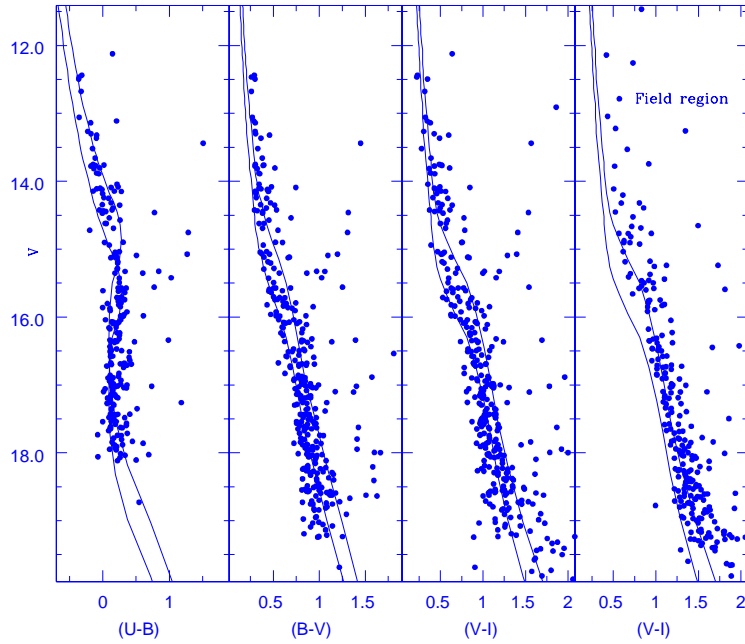


**Figure 5.** The  $V$ ,  $(U - B)$ ;  $V$ ,  $(B - V)$   $V$  and  $V$ ,  $(V - I)$  CM diagrams for the stars within the cluster radius and  $V$ ,  $(V - I)$  CM diagram for the field region. Solid lines represent the blue and red envelope of the cluster MS. The red envelope is determined by shifting the blue envelope vertically by 0.80 mag.

**Table 5.** A comparison of the colour excess ratios with  $E(B - V)$  with the normal interstellar extinction law given by Cardelli et al. (1989).

Object	$\frac{E(U-B)}{E(B-V)}$	$\frac{E(V-R)}{E(B-V)}$	$\frac{E(V-I)}{E(B-V)}$
Normal interstellar	0.72	0.65	1.25
NGC 2421	$0.73 \pm 0.06$	$0.54 \pm 0.08$	$1.25 \pm 0.11$

desired stars. In the absence of spectral class information, we determined their intrinsic colour using  $UBV$  photometric Q-method (cf. Johnson & Morgan (1953)) and the calibrations provided by Caldwell et al. (1993) for  $(U - B)_0$ ,  $(V - R)_0$  and  $(V - I)_0$  with  $(B - V)_0$ . Table 5 lists the mean values of the colour excess ratios. These values indicate that law of interstellar extinction is normal in the direction of the cluster.

### 3.4 Interstellar extinction in near-IR

Two Micron All Sky Survey (2MASS)  $JHK_s$  data is available for 180 stars in this cluster and has been used for determining the interstellar extinction in the direction of the cluster in near-IR. The data is complete up to 16.0 mag in  $J$ , 15.5 mag  $H$  and 15.0 mag in  $K_s$ . The  $K_s$  magnitude are converted into  $K$  magnitude following Persson et al. (1998). By combining optical and near-IR data, we plotted  $(J - K)$  versus  $(V - K)$  diagram in Fig 7. The ZAMS shown by

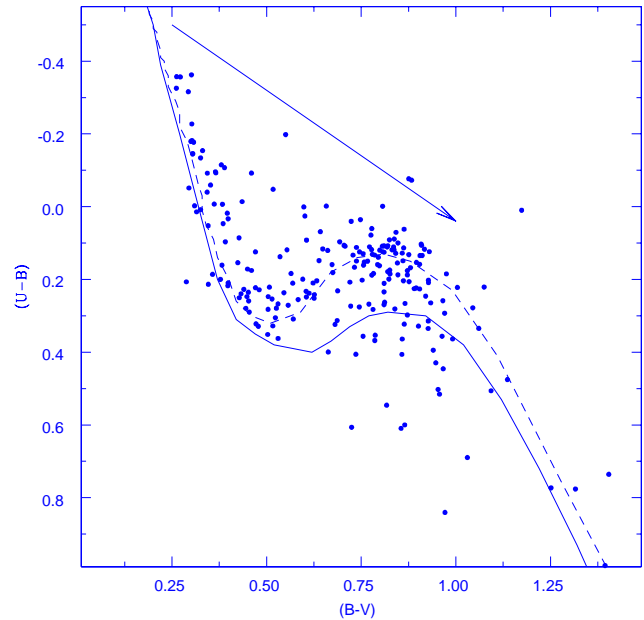


**Figure 6.** The  $(U - B)$  versus  $(B - V)$  colour-colour diagram of the cluster. The continuous straight line represents slope 0.72 and the direction of reddening vector while continuous curve represents locus of Schmidt-Kaler's (1982) ZAMS for solar metallicity. The curve shown by short dashed lines is the ZAMS given by Bertelli et al. (1994) for  $Z = 0.004$

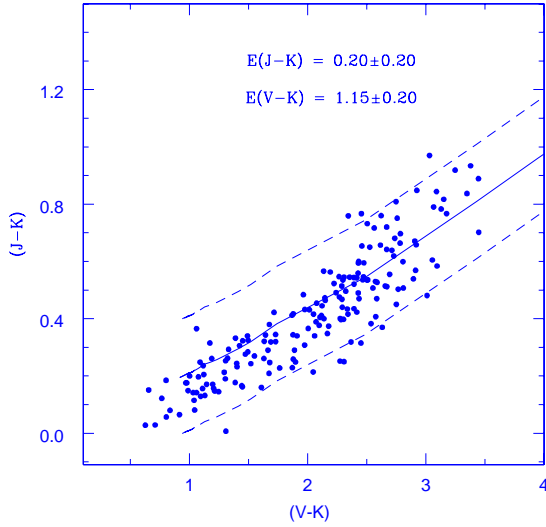


**Figure 7.** The plot of  $(J - K)$  versus  $(V - K)$  colour-colour diagram of the cluster for the stars within the cluster radius. The solid line is the ZAMS of  $Z = 0.004$  fitted for the marked values of the excesses while short dash lines show the errorbars.

solid line is taken from Bertelli et al. (1994) for  $Z = 0.004$ . The fit of ZAMS provides  $E(J - K) = 0.20 \pm 0.20$  mag and  $E(V - K) = 1.15 \pm 0.20$  mag for the cluster. The ratio  $\frac{E(J-K)}{E(V-K)} \sim 0.18 \pm 0.30$  is in good agreement with the normal interstellar extinction value 0.19 suggested by Cardelli et al. (1989).

### 3.5 Colour excess diagram

In Fig 8, we plotted colour-excess diagram for study of interstellar extinction law using optical and near-IR data. Colour excesses have been determined by comparing the observed colours of the stars earlier than A0 spectral type (see Sec. 3.3) with its intrinsic colours derived from the colour relation given by FitzGerald (1970) for  $(U - B)$  and  $(B - V)$ ; by Johnson (1966) for  $(V - R)$  and  $(V - I)$  and by Koornneef (1983) for  $(V - J)$ ,  $(V - H)$  and  $(V - K)$ . The colour excesses  $E(U - B)$ ,  $E(B - V)$ ,  $E(V - R)$ ,  $E(V - I)$ ,  $E(V - H)$ , and  $E(V - K)$  are plotted against  $E(V - J)$  in Fig 8. The solid straight line shown in this figure is the least square linear fits to the data point. In all the colour-excess diagrams except  $E(U - B)$  vs  $E(V - J)$  and  $E(B - V)$  vs  $E(V - J)$ , the values of correlation coefficient ( $r$ ) and fit indicate that the data points are well represented by linear relation. In  $E(U - B)$  vs  $E(V - J)$  and  $E(B - V)$  vs  $E(V - J)$  colour excess diagrams, scattering is more pronounced in the colour excess  $E(U - B)$  and  $E(B - V)$ . In Table 6, we have listed the slope of these straight lines which represent the reddening directions in the form of colour excess ratios. The colour excess ratios given by Cardelli et al. (1989) for normal interstellar

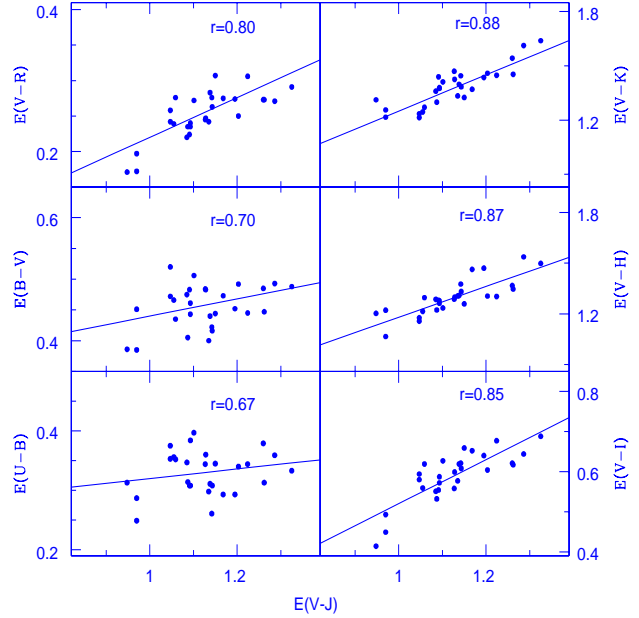


**Figure 8.** The plot of  $E(U - B)$ ,  $E(B - V)$ ,  $E(V - R)$ ,  $E(V - I)$ ,  $E(V - H)$ ,  $E(V - K)$  versus  $E(V - J)$ , colour excess diagram of the cluster. The solid straight lines represent the least square linear fit to the data point while  $r$  denotes its correlation coefficients.

matter are also listed in this Table. The present reddening directions generally agree within  $3\sigma$  with those given for the normal interstellar extinction law. This indicates that the interstellar extinction law is normal in the direction of the cluster.

Furthermore, to know about the nature of interstellar extinction law in the direction of the cluster, we have determined the value of  $R$ . We used the relation  $R = 1.1E(V - K)/E(B - V)$  given by Whittet & Breda (1980) which is generally used for the longer wavelengths. In this way we determined the value of  $R = 3.2 \pm 0.3$  which is in agreement with the value 3.1 for normal extinction law.

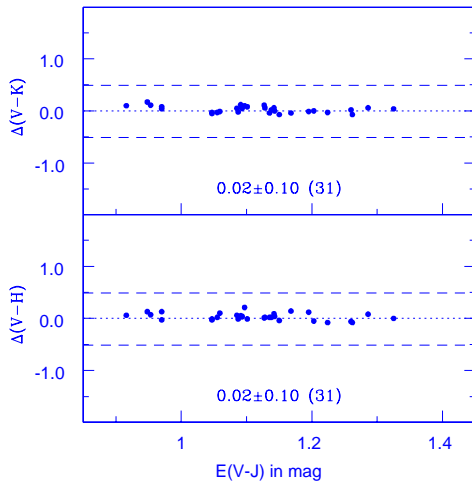
On the basis of above analysis, we can conclude that interstellar extinction law is normal in the direction of the cluster and is in agreement with our earlier result.

### 3.6 Near-IR excess fluxes

To study the near-IR flux in the stars, we plot  $\Delta(V - H)$  and  $\Delta(V - K)$  versus  $E(V - J)$  in Fig. 9. The value of  $\Delta(V - H)$  and  $\Delta(V - K)$  has been calculated by taking difference between the observed colour excess in  $(V - H)$  and  $(V - K)$  based on spectral type and the derived colour excess from  $E(V - J)$  assuming normal interstellar extinction law. The possible source of errors may be the observational uncertainties in  $JHK$  magnitudes, inaccuracies in the estimation of  $E(V - J)$  and in its ratio with  $E(V - H)$  and  $E(V - K)$ ; and errors in the spectral and luminosity classifications. Consequently, the differences can be considered statistically significant only if their absolute values are larger

**Table 6.** A comparison of extinction law in the direction of cluster with normal extinction law given by Cardelli et al. (1989).

Objects	$\frac{E(U-B)}{E(V-J)}$	$\frac{E(B-V)}{E(V-J)}$	$\frac{E(V-R)}{E(V-J)}$	$\frac{E(V-I)}{E(V-J)}$	$\frac{E(V-H)}{E(V-J)}$	$\frac{E(V-K)}{E(V-J)}$	$\frac{E(J-K)}{E(V-K)}$
Normal value	0.32	0.43	0.27	0.56	1.13	1.21	0.19
NGC 2421	0.10±0.09	0.14±0.10	0.28±0.05	0.55±0.08	0.98 ±0.13	1.08±0.12	0.18±0.30


**Figure 9.** The plot of  $\Delta(V-H)$  and  $\Delta(V-K)$  versus  $E(V-J)$ . The horizontal dotted lines denote zero excess while short dashed lines denote the extent of the expected errors.

than  $\sim 0.5$  mag. Fig. 9 gives an indication that for all the stars the values of  $\Delta(V-H)$  and  $\Delta(V-K)$  are close to zero. Hence, we can conclude that near-IR fluxes are not seen in any of the star under study indicating absence of gas and dust envelope around them.

### 3.7 Distance to the cluster

The distance of the cluster is determined by fitting the ZAMS. The intrinsic CM diagram of the cluster is depicted in Fig. 10. In order to reduce the field star contamination, we have used only those probable cluster members which are within the cluster radius and photometric members (see Sec. 3.2). For converting apparent  $V$  magnitude and  $(U-B)$ ,  $(B-V)$ ,  $(V-R)$  and  $(V-I)$  colours into intrinsic one, we used average values of  $E(B-V)$  and following relations for  $E(U-B)$  (cf. Kamp 1974),  $A_V$  and  $E(V-I)$  (Walker 1987) and  $E(V-R)$  (Alcalá et al. 1988).

$$E(U-B) = [X + 0.05E(B-V)]E(B-V)$$

where  $X = 0.62 - 0.3(B-V)_0$  for  $(B-V)_0 < -0.09$   
and  $X = 0.66 + 0.08(B-V)_0$  for  $(B-V)_0 > -0.09$

$A_V = [3.06 + 0.25(B-V)_0 + 0.05E(B-V)]E(B-V)$ ;  
and  $E(V-R) = [E1 + E2E(B-V)]E(B-V)$

where  $E1 = 0.6316 + 0.0713(B-V)_0$   
and  $E2 = 0.0362 + 0.0078(B-V)_0$ ;

$E(V-I) = 1.25[1 + 0.06(B-V)_0 + 0.014E(B-V)]E(B-V)$

The ZAMS taken from Bertelli et al. (1994) for  $Z = 0.004$  is plotted in  $V_0$ ,  $(U-B)_0$ ;  $V_0$ ,  $(B-V)_0$ ;  $V_0$ ,  $(V-R)_0$  and  $V_0$ ,  $(V-I)_0$  diagrams. The visual fit of the ZAMS to the bluest envelope of intrinsic CM diagrams provides  $(m-M)_0 = 11.7 \pm 0.2$  mag for the cluster NGC 2421. The distance value of the cluster should be reliable since it has been derived by fitting the ZAMS over a wide range of MS. The distance modulus determined above gives a distance of  $2.2 \pm 0.2$  Kpc for the cluster. Our derived value of the distance is not very much different from the value 1.9 Kpc derived by Moffat & Vogt (1975) while it is less than the value 2.8 Kpc derived by Ramsay & Pollacco (1992).

### 3.8 Age of the cluster

The age of the cluster is determined by comparing the theoretical stellar evolutionary isochrones given by Bertelli et al. (1994) for  $Z = 0.004$  with its intrinsic CM diagram (Fig. 10). The isochrones include the effect of mass loss and convective core overshooting in the model. We have fitted the isochrones of  $\log(\text{age}) = 7.8, 7.9$  and  $8.0$  to the intrinsic CM diagrams. The isochrones fitted to the brighter stars indicate that age of the cluster is  $80 \pm 20$  Myr.

To derive the age and distance of the cluster with the combination of optical and near-IR data, we plot  $V$  versus  $(V-K)$  and  $K$  versus  $(J-K)$  CM diagram in Fig 11. The theoretical isochrones given by Bertelli et al. (1994) for  $Z = 0.004$  and  $\log(\text{age}) = 8.0$  have been overplotted in the CM diagram. The apparent distance moduli  $(m-M)_{V,(V-K)}$  and  $(m-M)_{K,(J-K)}$  turn out to be  $13.0 \pm 0.3$  and  $11.8 \pm 0.3$  mag for this cluster. Using the reddening values estimated in Sec. 3.4, we derived a distance of  $2.3 \pm 0.3$ . Both age and distance determination for the cluster are thus in agreement with our earlier estimates. However, scattering is larger due to the large errors in  $JHK$  mags.

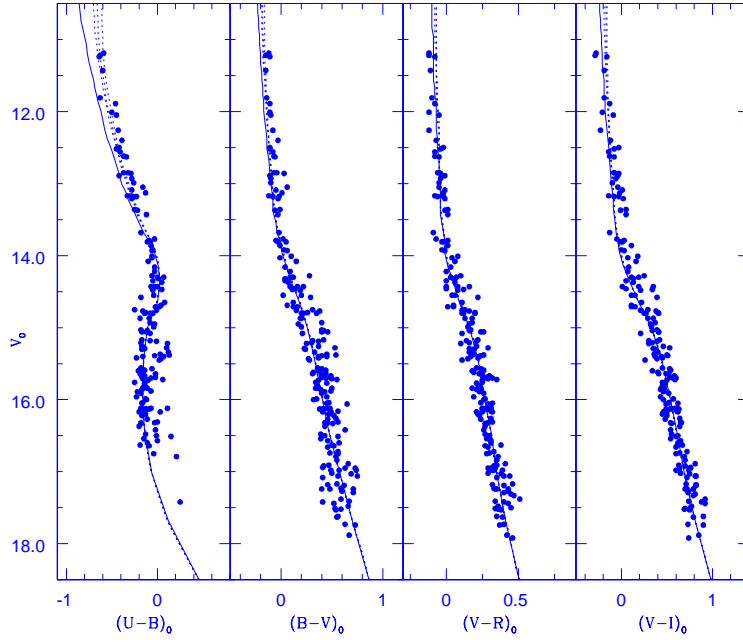


**Figure 10.** The intrinsic colour-magnitude diagram of the cluster. The continuous solid line curve are the ZAMS given by Bertelli et al. (1994) for  $Z = 0.004$ . The short dashed line curve are the isochrones taken from Bertelli et al. (1994) for  $Z = 0.004$  and  $\log(\text{age}) = 7.8, 7.9$  and  $8.0$ .

**Table 7.** Variation of completeness factor (CF) in the  $V$ ,  $(V - I)$  diagram with the MS brightness.

$V$ mag range	CF
12 - 13	0.99
13 - 14	0.99
14 - 15	0.99
15 - 16	0.96
16 - 17	0.94
17 - 18	0.93
18 - 19	0.93

### 3.9 Luminosity and Mass function

To determine the luminosity function of the cluster, we considered  $V$  versus  $(V - I)$  CM diagram in comparison to others because it is deepest. For removing the field star contamination, we adopted the photometric criteria by defining the blue and red envelope for the MS (see Sec. 3.2). The same envelope is also drawn for the  $V$  versus  $(V - I)$  CM diagram of the field region. Stars are counted within this envelope, for both the cluster and the field region CM diagrams. The observed cluster luminosity function is the difference between the counts in the two fields after accounting for the difference in area between the cluster and field regions.

Incompleteness corrections are handled by introducing a number of artificial stars into the original data images of  $V$  and  $I$  passband. The method used for this has been described in Yadav & Sagar (2002), so we present only the results here. Table 7 shows the completeness factor in the

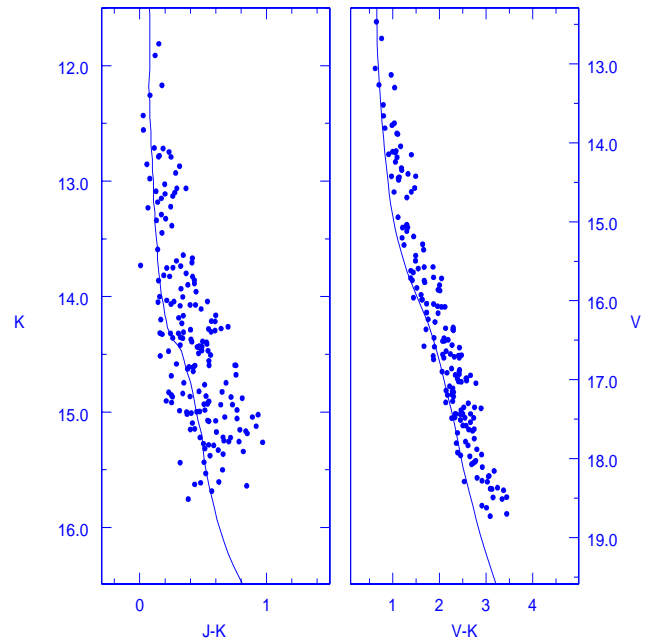


**Figure 11.** The  $K$  versus  $(J - K)$  and  $V$  versus  $(V - K)$  CM diagrams of the cluster using probable cluster members. The solid curve represent the isochrones of  $\log(\text{age}) = 8.0$  taken from Bertelli et al. (1994) for  $Z = 0.004$ .

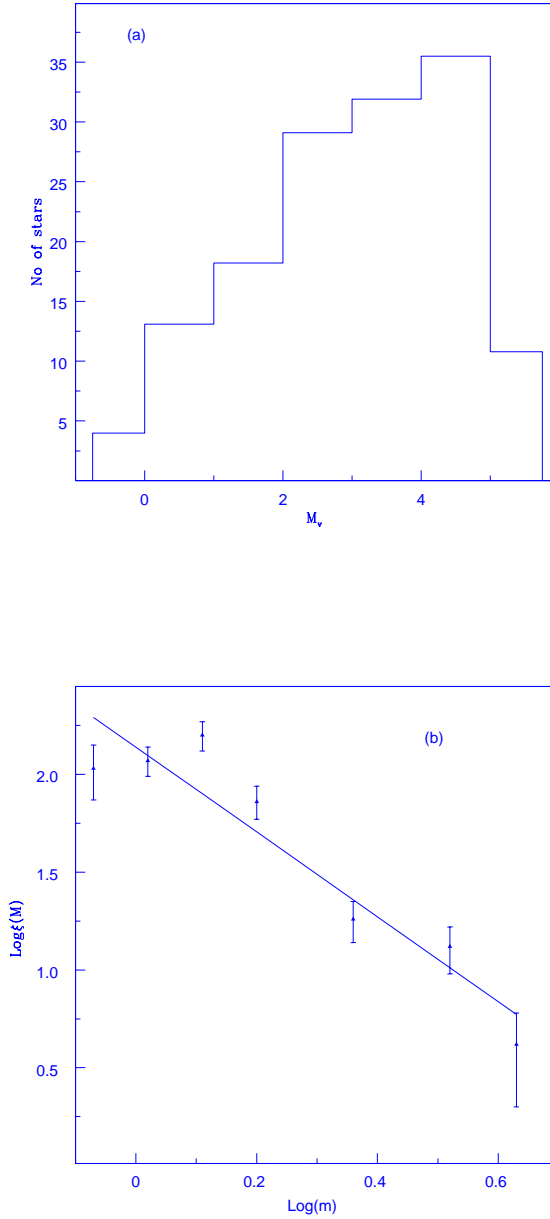


**Figure 12.** (a) Luminosity function of the cluster. (b) Mass function derived using Bertelli et al. (1994) isochrones.

cluster region. To summarize, the completeness in the cluster region for MS stars is found to be 93.0% at  $V = 19.0$  mag. The completeness in the field region has been considered as 100%.

The final corrected star counts are found by applying the incompleteness corrections in the cluster region. Fig. 12(a) shows the final luminosity function for the cluster NGC 2421. The luminosity function of the cluster rises until  $M_v = 4.5$  and then decreases.

The mass function (MF) can be derived by using the relation  $\log \frac{dN}{dM} = -(1+x) \times \log(M) + \text{constant}$ , where  $dN$  rep-

resents the number of stars in a mass bin  $dM$  with central  $M$  and  $x$  is the slope of MF. In transferring the LF to the MF, we need theoretical evolutionary tracks and accurate knowledge of cluster parameters like reddening, distance, age, etc. Theoretical models given by Bertelli et al. (1994) has been used to convert LF to MF and the resulting MF is shown in Fig. 12(b). The derived slope of the MF is  $x = 1.2 \pm 0.3$  is in agreement within the error with the value 1.35 given by Salpeter (1955) for the Solar neighbourhood stars.

### 3.10 Dynamical state and Mass segregation

In the lifetime of a star cluster, encounters between its member stars gradually lead to an increased degree of energy equipartition throughout the cluster. The most significant consequence of this process is that the higher-mass cluster stars gradually sink towards the cluster center and in the process transfer their kinetic energy to the more numerous lower-mass stellar component, thus leading to mass segregation. The time-scale on which a cluster will have lost all traces of its initial conditions is well represented by relaxation time  $T_E$ . It is given by

$$T_E = \frac{8.9 \times 10^5 N^{1/2} R_h^{3/2}}{\langle m \rangle^{1/2} \log(0.4N)}$$

where  $N$  is the number of cluster members,  $R_h$  is the half-mass radius of the cluster and  $\langle m \rangle$  is the mean mass of the cluster stars (cf. Spitzer & Hart 1971). The value of  $R_h$  has been assumed as half of the cluster radius derived by us. Using distance, the angular value of the radius has been converted into linear value. The probable cluster members are selected using CM diagram of the cluster after removing the field star contamination and applying data incompleteness corrections. In this way, we estimated the dynamical relaxation time  $T_E = 30$  Myr for this cluster which implies that the cluster age is 2.6 times its relaxation age. Therefore, we can conclude that the cluster is dynamically relaxed.

To investigate sign of mass segregation, we split the cluster members in three mass range  $4.7 \leq M_\odot < 3.4$ ,  $3.4 \leq M_\odot < 2.1$  and  $2.1 \leq M_\odot \leq 0.8$ . Fig. 13 shows the cumulative radial stellar distribution of stars for different masses. To examine the distribution of stars whether they belong to the same distribution or not, we performed K-S test among these distribution. The K-S test provides sign of mass segregation at confidence level of 85%. In the previous paragraph, we have seen that this cluster is dynamically relaxed and hence one of the possible cause of mass segregation may be the dynamical evolution of the cluster.

## 4 CONCLUSIONS

We have investigated the area of open cluster NGC 2421 using  $UBVRI$  CCD and  $2MASS JHK_s$  data. The main results of our analysis are the following.

(i) The radius of the cluster is determined as  $3'.0$  which corresponds to 1.9 pc at the distance of the cluster.

(ii) We estimated the abundance of the cluster stars as  $Z = 0.004$  using excess in  $(U - B)$ . The  $(U - B)$  versus  $(B - V)$  colour-colour diagram yields  $E(B - V) = 0.42 \pm 0.05$ . The analysis of  $JHK$  data in combination with the optical

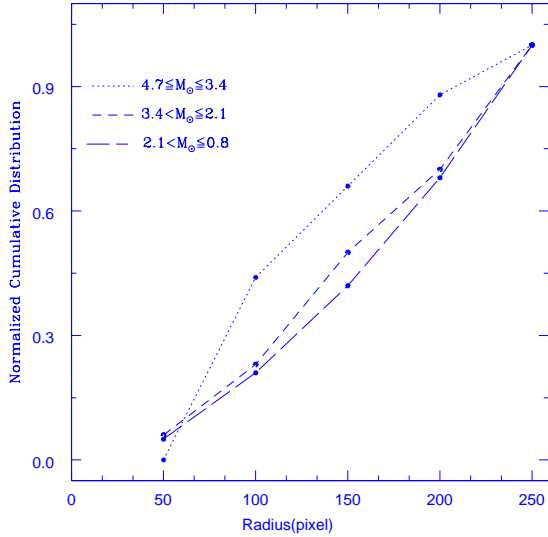


**Figure 13.** The cumulative radial distribution of stars in various mass range.

data provide  $E(J - K) = 0.20 \pm 0.20$  mag and  $E(V - K) = 1.15 \pm 0.20$  mag. Our analysis shows that interstellar extinction law is normal towards the cluster direction. No stars found which are having near-IR fluxes due to the presence of circumstellar material around them.

(iii) A ZAMS fitting procedure gives a distance of  $2.2 \pm 0.2$  Kpc for this cluster which is also supported by the value of  $2.3 \pm 0.3$  Kpc determined by us using the optical and near-IR data. An age of  $80 \pm 20$  Myr is determined using the isochrones of  $Z = 0.004$  given by Bertelli et al. (1994).

(iv) The mass function slope  $x = 1.2 \pm 0.3$  is derived by considering the corrections of field star contamination and data incompleteness. Our analysis indicate that the cluster NGC 2421 is dynamically relaxed and one plausible reason of this relaxation may be the dynamical evolution of the cluster.

## ACKNOWLEDGEMENTS

We thank the referee for valuable comments, which have improved the quality of this paper. This study made use of 2MASS and WEBDA.

## REFERENCES

- Alcalá, J. M., Ferro, A. A., 1988, *Rev. Mex. Astro. Astrofis*, 16, 81  
 Bertelli, G., Bressan, A., Chiosi, C., Fagotto, F., Nasi, E., 1994, *A&AS*, 106, 275  
 Caldwell, A. R. John, Cousins, A. W. J., Ahlers, C. C., Wamelen, P. van, Maritz, E. J., 1993, *SAAO Circ. No. 15*  
 Cardelli, J. A., Clayton, G. C., Mathis, J. S., 1989, *ApJ*, 345, 245  
 Carney, B. W., 1979, *ApJ*, 233, 211  
 FitzGerald, M. P., 1970, *A&A*, 4, 234

- Johnson, H. L., Morgan, W. W., 1953, *ApJ*, 117, 313  
 Johnson, H. L., Morgan, W. W., 1966, *ARA&A*, 4, 193  
 Kamp, L. W., 1974, *A&AS*, 16, 1  
 Koornneef, J., 1983, *A&A*, 128, 84  
 Landolt, A. U., 1992, *AJ*, 104, 340  
 Merrelliod, J. C., 1995, in *Information and on - line data in Astronomy*, Eds E. Egret and M. A. Abrecht, Kulwer Academic Press, p 227.  
 Moffat, A. F. J., Vogt, N. 1975, *A&AS*, 20, 85  
 Persson, S. E., Murphy, D. C., Krzeminski, W., Roth, M., & Rieke, M. J., 1998, *AJ*, 116, 2475  
 Ramsay, G., Pollacco, D. L., 1992, *A&AS*, 94, 73  
 Ruprecht, J. 1966, *Bull. Astron. Inst. Czech.*, 17, 33  
 Salpeter, E. E., 1955, *ApJ*, 121, 161  
 Schmidt - Kaler Th., 1982, In: *Landolt/Bornstein, Numerical Data and Functional Relationship in Science and Technology*, New series, Group VI, Vol. 2b, Scaifers K. & Voigt H. H. (eds.) Springer - Verlag, Berlin, p. 14  
 Spitzer, L. & Hart, M. H., 1971, *ApJ*, 164, 399  
 Stetson, P. B., 1987, *PASP*, 99, 191  
 Stetson, P. B., 1992, in *Warrall D. M., Biemesderfer C., Barnes J. eds., ASP Conf. Ser. Vol. 25, Astronomical Data Analysis Software and System I. Astron. Soc. Pac., San Francisco*, p. 297  
 Walker, A. R., 1987, *MNRAS*, 229, 31  
 Whittet, D. C. B., van Breda, I. G., 1980, *MNRAS*, 192, 467  
 Yadav, R. K. S. and Sagar, R., 2002, *MNRAS*, 337, 133